

Dramatic Plasmon Response to the Charge-Density-Wave Gap Development in 1T-TiSe₂

Zijian Lin,^{1,2,*} Cuixiang Wang^{1,2,*}, A. Balassis,³ J. P. Echeverry⁴, A. S. Vasenko,^{5,6} V. M. Silkin,^{7,8,9}
E. V. Chulkov,^{7,8,5} Youguo Shi,^{1,10} Jiandi Zhang,¹ Jiandong Guo,^{1,2,10,†} and Xuetao Zhu^{1,2,10,‡}

¹Beijing National Laboratory for Condensed Matter Physics and Institute of Physics,
Chinese Academy of Sciences, Beijing 100190, China

²School of Physical Sciences, University of Chinese Academy of Sciences, Beijing 100049, China

³Department of Physics and Engineering Physics, Fordham University,
441 East Fordham Road, Bronx, New York 10458, USA

⁴Universidad de Ibagué Carrera 22 Calle 67 B, Av. Ambalá Ibagué Tolima 730007, Colombia

⁵HSE University, 101000 Moscow, Russia

⁶I. E. Tamm Department of Theoretical Physics, P. N. Lebedev Physical Institute,
Russian Academy of Sciences, 119991 Moscow, Russia

⁷Donostia International Physics Center (DIPC), 20018 San Sebastián/Donostia, Basque Country, Spain

⁸Departamento de Polímeros y Materiales Avanzados: Física, Química y Tecnología, Facultad de Ciencias Químicas,
Universidad del País Vasco UPV/EHU, Apartado 1072, 20080 San Sebastián/Donostia, Basque Country, Spain

⁹IKERBASQUE, Basque Foundation for Science, 48013 Bilbao, Basque Country, Spain

¹⁰Songshan Lake Materials Laboratory, Dongguan, Guangdong 523808, China

 (Received 30 December 2021; revised 20 April 2022; accepted 29 September 2022; published 24 October 2022)

1T-TiSe₂ is one of the most studied charge density wave (CDW) systems, not only because of its peculiar properties related to the CDW transition, but also due to its status as a promising candidate of exciton insulator signaled by the proposed plasmon softening at the CDW wave vector. Using high-resolution electron energy loss spectroscopy, we report a systematic study of the temperature-dependent plasmon behaviors of 1T-TiSe₂. We unambiguously resolve the plasmon from phonon modes, revealing the existence of Landau damping to the plasmon at finite momentums, which does not support the plasmon softening picture for exciton condensation. Moreover, we discover that the plasmon lifetime at zero momentum responds dramatically to the band gap evolution associated with the CDW transition. The interband transitions near the Fermi energy in the normal phase are demonstrated to serve as a strong damping channel of plasmons, while such a channel in the CDW phase is suppressed due to the CDW gap opening, which results in the dramatic tunability of the plasmon in semimetals or small-gap semiconductors.

DOI: 10.1103/PhysRevLett.129.187601

In charge-density-wave (CDW) material, the CDW gap development, which is often served as the order parameter to characterize the CDW transition [1,2], can strongly influence the emergent phenomena of the system. 1T-TiSe₂, a quasi-two-dimensional layered material, undergoes a three-dimensional second-order CDW transition at $T_c \sim 200$ K with $\mathbf{q}_{\text{CDW}} = (1/2, 0, 1/2)$ [3]. The CDW origin of 1T-TiSe₂ was described by several different mechanisms [3–5]. One of the most-studied scenarios is the electron-phonon coupling [4,6–13], which is the CDW origin in many quasi-two-dimensional systems [2]. On the other hand, the CDW order in 1T-TiSe₂ is proposed to be induced by the formation of the exciton insulator (EI) [14–21]. And some recent studies claimed that the EI and the electron-phonon coupling may cooperatively induce the CDW transition [22–27].

Understanding the band structure evolution is essential for identifying the origin of the CDW transition [28,29]. In the normal phase above T_c [Fig. 1(a)], 1T-TiSe₂ is a semiconductor with a small indirect gap [28] (or a

semimetal with a small band overlap [9]), where the bottom of the conduction band is almost tangent to the Fermi level E_F [30,31]. Interestingly, there exists a CDW fluctuating band above T_c [7,8,14,32,33], which may provide a precursor of the CDW gap [34]. In the CDW phase below

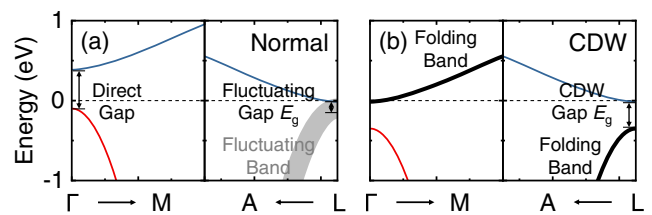


FIG. 1. Schematics of the band structure in 1T-TiSe₂. (a) Band structure in the normal phase. The red and blue lines represent the valence and conduction bands, respectively. The fluctuating band is represented by the gray shadow. The dashed lines indicate the Fermi level. (b) Band structure in the CDW phase. Black lines represent the folding bands due to the distortion.

T_c [Fig. 1(b)], the gap opens by the valence band gradually shifting toward higher binding energy, leaving the conduction band still tangent to E_F and accompanied by a CDW band folding [8,9,15,16,32]. Because of the coexistence of the metallic nature and CDW gap in both the normal and CDW phases, the plasmon provides a good window into visualizing the effect of the CDW gap development on the electronic properties. Recently, the plasmon softening at q_{CDW} around T_c was proposed to serve as the signature of the EI [21]. However, a recent theoretical study attributed the seeming plasmon softening signal to the interband transitions [35].

In this Letter, using the momentum-resolved high-resolution electron energy loss spectroscopy (HREELS) with the capability of two-dimensional energy-momentum mapping [36], we systematically measured the plasmon behaviors in $1T$ -TiSe₂. Our results unambiguously resolve the plasmon from phonon modes and demonstrate the existence of Landau damping [37–39] to the plasmon at finite momenta within the full temperature range, revealing that there is no plasmon softening at q_{CDW} . Extraordinarily, we discover that the plasmon at zero momentum responds to the CDW transition dramatically, from a broad feature covering the energy of 50–150 meV to

a sharp feature with the well-defined resonant frequency at ~ 50 meV in the low-temperature CDW phase. Such wide-range tunability is attributed to the gap opening associated with the CDW transition that suppresses the interband damping channels of the plasmon.

Temperature-dependent HREELS results.—The measurements were performed on cleaved $1T$ -TiSe₂ single-crystalline samples *in situ* in a HREELS system with reflected scattering geometry. The detailed experimental methods and sample characterizations are described in the Supplemental Material [40]. The HREELS data were collected with the sample temperature varying from 35 to 300 K along the two high symmetry directions $\bar{\Gamma}$ - \bar{M} and $\bar{\Gamma}$ - \bar{K} in the surface Brillouin zone (BZ). The incident electron beam energy E_i from 7 to 110 eV (110 eV data presented in the main paper, while others in the Supplemental Material [40]) is used, with a typical energy resolution of 3 meV. Figure 2 shows the HREELS results of $1T$ -TiSe₂ at various temperatures. The temperature-dependent E - $q_{//}$ mappings ($q_{//}$ denotes the momentum parallel to the surface) along the $\bar{\Gamma}$ - \bar{M} and $\bar{\Gamma}$ - \bar{K} directions are presented in Figs. 2(a)–2(d).

In HREELS, the strong intensity distributions near the $\bar{\Gamma}$ point are dominated by the dipole scattering, and the

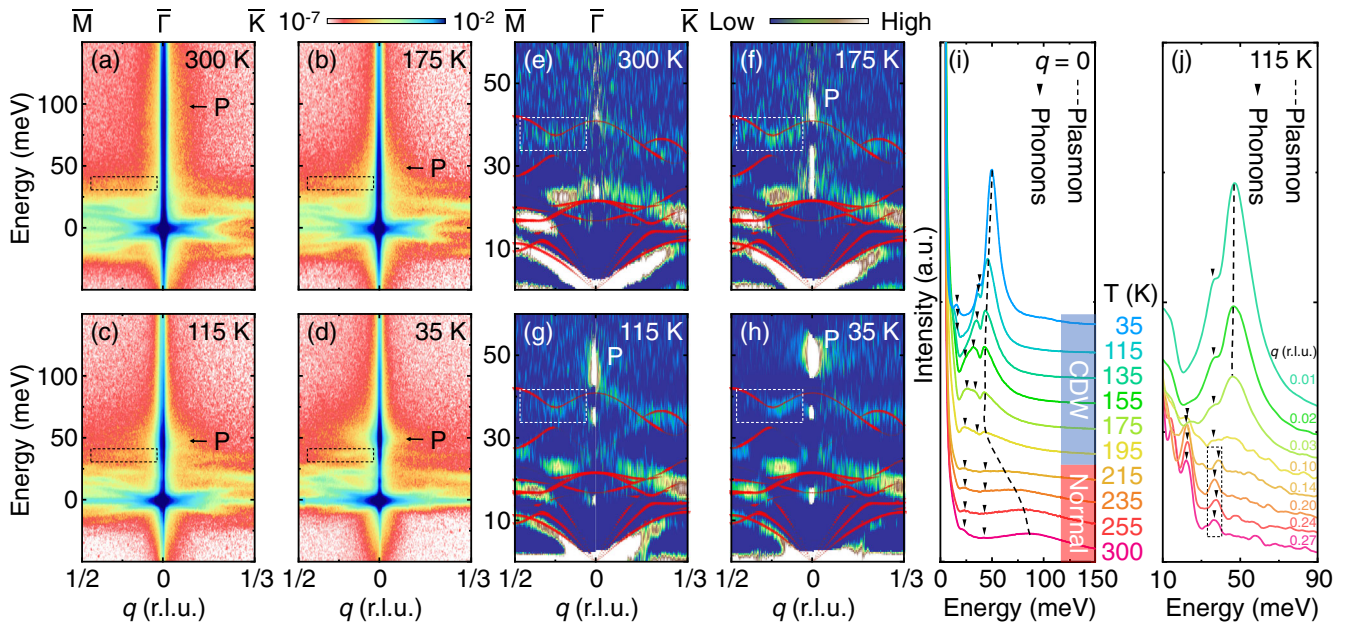


FIG. 2. Temperature (T)-dependent HREELS results in $1T$ -TiSe₂. (a)–(d) E - $q_{//}$ mappings of HREELS at 300, 175, 115, and 35 K, respectively. At the $\bar{\Gamma}$ point, the plasmon is labeled by P . Dashed-line rectangles show the typical unchanged phonon dispersions close to the plasmon. The momenta are represented in the form of $(q, 0)$ and (q, q) along $\bar{\Gamma}$ - \bar{M} and $\bar{\Gamma}$ - \bar{K} directions with the reciprocal lattice unit (r.l.u.) as the unit. The color scale corresponds to the logarithmic intensity. The positive and negative energy ranges represent the Stokes and anti-Stokes scatterings, respectively. (e)–(h) Second differential images of (a)–(d), respectively. The red triangles are the surface phonon dispersions calculated by the slab method. The size of the triangles indicates the spectral weight of the surface amplitude of phonons. White dashed-line rectangles are the same as the dashed-line rectangles in (a)–(d). (i) Stack of the energy distribution curves (EDCs) at the $\bar{\Gamma}$ point at different temperatures. The triangles and dashed lines are guides to the eyes of phonons and the plasmon, respectively. (j) Stack of the EDCs at 115 K at different q 's. The intensities of EDCs at $q = 0.01, 0.02,$ and 0.03 r.l.u. is multiplied by $0.03, 0.08,$ and 0.2 for better presentation, respectively. The dashed-line rectangle is the same as the dashed-line rectangles in (a)–(d).

relatively weak features away from the $\bar{\Gamma}$ point to the BZ boundary correspond to the impact scattering regime [55]. Then, it is obvious that there are two kinds of distinct energy loss features divided by the energy of 45 meV at 300 K. The loss features higher than 45 meV, labeled as P , are only located near the $\bar{\Gamma}$ point, which are pure dipole scattering features and regarded as the plasmon originating from the charge carrier both in the normal and CDW phases [56,57]. The loss features lower than 45 meV exist throughout the BZ, which are typical impact scattering signals from phonons [55]. To show their dispersions more clearly, Figs. 2(e)–2(h) display the second differential images of the original spectra superimposed on the calculated surface phonon dispersions (red triangles) using an 11-layer slab model (see the details in the Supplemental Material [40]). Overall, the calculated phonon dispersions, especially the optical phonon branches, match well with the experimental results.

The evolution of the plasmon with temperature is illustrated by a stacking plot of the loss features at the $\bar{\Gamma}$ point [Fig. 2(i)]. As the temperature decreases from 300 K to T_c , the energy of the plasmon gets closer to the optical phonon. When the temperature further decreases below T_c , the energy of the plasmon slightly increases, and the linewidth of the plasmon changes dramatically. These phenomena will be discussed later in more detail.

Compared with the previous HREELS study in Ref. [21], our results show similar temperature-dependent plasmon behavior at the $\bar{\Gamma}$ point, but surprisingly, we did not observe the plasmon softening at q_{CDW} . In our energy-momentum mappings at any temperature, the plasmon only exists near the $\bar{\Gamma}$ point and does not disperse to the low-energy range at the BZ boundary. In detail, Fig. 2(j) shows dispersion behaviors of the plasmon and phonons in the q space along the $\bar{\Gamma}$ - \bar{M} direction [58]. The plasmon decays from a sharp peak at $q = 0.01$ r.l.u. to a weaker peak at $q = 0.03$ r.l.u. As q increases, the plasmon is not a well-defined peak anymore at $q = 0.10$ r.l.u. and disappears (indistinguishable from noise) beyond $q = 0.14$ r.l.u. The reported energy loss signal over the entire BZ at 17 K in Ref. [21], interpreted as a dispersionless plasmon, could be from diffusion scattering [55]. In our results, the delicate optical phonon dispersions [those highlighted by the dashed-line rectangles in Fig. 2], which were not observed in Ref. [21], can be clearly resolved from the plasmon. The energy range of these optical phonon branches is close to the claimed softening plasmon energy, so the softening plasmon dispersion around T_c [21] seems to be from the envelope of phonon signals. Details of the comparison are described in the Supplemental Material [40].

Landau damping of the plasmon.—The observed plasmon damping behaviors can be well understood by the calculations of the loss functions, which were carried out in the framework of time-dependent density functional theory (see details in the Supplemental Material [40]).

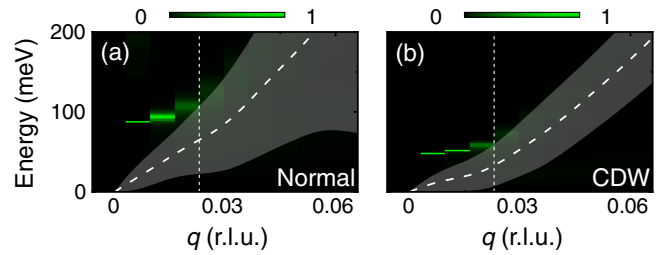


FIG. 3. Theoretical SPE in $1T$ -TiSe₂. (a) and (b) Calculated loss function mappings of the normal and CDW state, respectively. The gray shadowed areas centered at thick white dashed lines are the calculated SPE regions. The green color mappings in loss functions are plasmons. Thin dashed lines highlight calculated critical momenta q_c .

For simplicity, the calculated band structure in the CDW phase does not include the effects of band folding and renormalization. The calculated single particle excitation (SPE) regions for the normal and CDW band structures are indicated by white dashed lines and shadow areas centered at thick white dashed lines in Fig. 3, and plasmon dispersions are represented by color mappings of the calculated loss functions. At the lowest q , plasmons are almost delta functions. However, plasmons broaden and weaken rapidly approaching SPE borders. Beyond the calculated $q_c = 0.024$ r.l.u. [59], plasmons are not well-defined collective excitations anymore due to the strong decay to SPEs. This explains the experimentally observed fast decay of the plasmon at small momentum.

Damping of the plasmon at the long wavelength limit.—Notice there is a dramatic change of plasmon behaviors across T_c at the long wavelength limit (near $q = 0$), especially the linewidth [Fig. 2(i)]. In the normal state, the relatively broad linewidth indicates the strong plasmon damping above T_c . In contrast, in the CDW state, the linewidth is much smaller, demonstrating that the plasmon damping is largely suppressed below T_c . Moreover, the calculated loss function near $q = 0$ is almost a delta function without any damping in Fig. 3 in both the normal and CDW phases, suggesting that an analysis beyond the framework used above (which excludes the CDW band folding) is necessary.

To characterize the temperature-dependent damping behavior at $q = 0$, we plotted the plasmon lifetime parameter $\tau_{\text{pl}} = (\Delta E_{\text{pl}}/E_{\text{pl}})^{-1}$ in Fig. 4(a), where E_{pl} and ΔE_{pl} are the energy and linewidth of the plasmon, respectively. The damping of the plasmon is slightly enhanced when the temperature decreases from room temperature toward T_c , and as the temperature drops further below T_c , the damping is substantially suppressed, and even becomes much weaker than that at 300 K. Meanwhile, we noticed that the lifetime of the plasmon and the CDW gap as the order parameter (adopted from the resonant inelastic X-ray scattering results [60]) have a synchronous temperature-dependent behavior, implying that the opening of the CDW

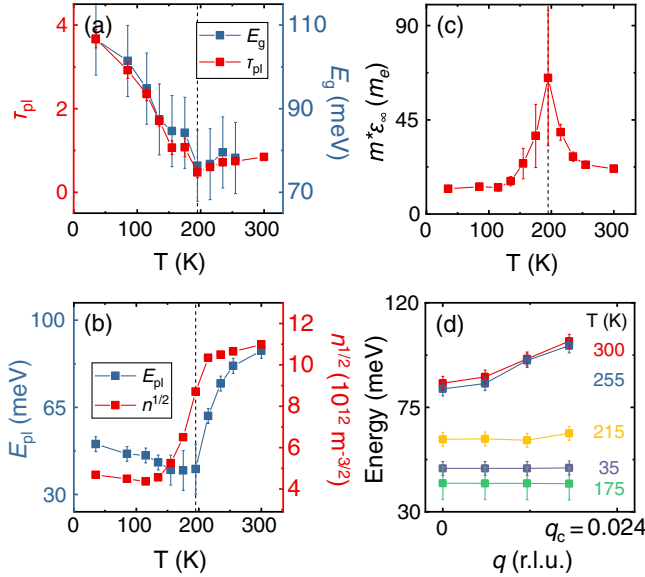


FIG. 4. Temperature-dependent plasmon features in 1T-TiSe₂. (a) Temperature dependence of the dimensionless lifetime parameter τ_{pl} of the plasmon and the CDW gap E_g in Ref. [60]. The dashed line highlights the T_c . (b) Temperature dependence of the plasmon energy E_{pl} and the square root of the carrier concentration $n^{1/2}$ in Ref. [61], respectively. (c) Temperature dependence of the multiplication of the effective carrier mass m^* and the high-frequency dielectric constant ϵ_∞ . The unit of the vertical axis (m_e) is the mass of free electrons. (d) Temperature dependence of the plasmon dispersion below q_c .

gap is connected to the enhancement of the plasmon lifetime, that is, the depression of the plasmon damping below T_c .

In classical dielectric theory, the effect of the gap (or interband transitions) on plasmons is approximated by the high-frequency dielectric constant ϵ_∞ , and the plasmon energy or frequency is given by $E_{pl} = \hbar\omega_{pl} = \hbar(ne^2/m^*\epsilon_\infty)^{1/2}$, where n , e , and m^* are the carrier concentration, the charge of an electron, and the effective electron mass, respectively. In Fig. 4(b), we compared the fitted plasmon energy at $q = 0$ from our experiment and the carrier concentration in Ref. [61]. Although both E_{pl} and $n^{1/2}$ as functions of temperature show abrupt changes at T_c , the discrepancy between them clearly indicates that, besides the carrier density, there must be other factors that are responsible for the evolution of the plasmon energy. We divided $(E_{pl}^2)^{-1}$ by n^{-1} to exclude the effect of the carrier concentration, and obtained the temperature dependence of the multiplication of ϵ_∞ and m^* [Fig. 4(c)]. The previous experiment [62] did not show an observable change of m^* near T_c , so the additional drop in plasmon energy compared to $n^{1/2}$ on cooling across T_c should be attributed to an abrupt increase in ϵ_∞ related to the CDW gap. Besides, the plasmon dispersion gradually flattens upon cooling, from a conventional parabolic shape in the normal phase to a dispersionless flat line in the CDW phase, as shown in Fig. 4(d).

Evolution of the plasmon with the CDW gap.—To explain the temperature-dependent plasmon features, we show a phenomenological model where the plasmon evolves with the development of the CDW gap. In this model, we employed a simple dielectric theory to simulate the influence of the interband transition across the CDW gap on the dispersion and damping of the plasmon. The dielectric function can be expressed as follows (see details in the Supplemental Material [40]):

$$\epsilon(q, \omega) = 1 - \frac{\omega_{pl}^2(q)}{\omega^2} + \frac{\omega_{intra}^2(q)}{\omega^2 - \omega_{intra}^2(q) + i\Gamma_{intra}\omega} + \frac{\omega_{pl}^2(q)}{\omega^2 - \omega_{CDW}^2(q) + i\Gamma_{CDW}\omega}.$$

The first two terms $\{1 - [\omega_{pl}^2(q)/\omega^2]\}$ represent a partly screened plasmon by the higher-energy interband transitions other than ones across the CDW gap. In this simulation, the plasmon dispersion $\omega_{pl}(q)$ follows a parabolic form (yellow lines in Fig. 5) in the random phase approximation. The third term represents the intraband transitions [i.e., the Landau damping in Fig. 3], where ω_{intra} corresponds to the SPE boundary [63], and Γ_{intra} is the linewidth of the intraband transitions. The above parameters in the plasmon and intraband terms are kept constant in this simulation. The last term represents the interband transitions purely originating from the CDW gap (blue lines in Fig. 5), where $\hbar\omega_{CDW}(q) = E_g + (E_F - E_{cb}) + C(q - k_F)^2$ with E_g the size of the gap, E_{cb} the energy of the conduction band bottom, and C the constant related to the band slope (see details in the Supplemental Material [40]). Γ_{CDW} is the linewidth of the interband transition across the CDW gap. The loss functions $\text{Im}[-\epsilon(q, \omega)^{-1}]$ are plotted in Fig. 5 with different CDW gap parameters.

In the normal phase, the lowest interband transition is contributed by the hopping from the CDW fluctuating band [7,8,14,32–34] to the conduction band at E_F [shown as Fig. 1(a)]. Referring to the resonant inelastic x-ray scattering results [60], we let $E_g = 50$ meV. At high temperature [Fig. 5(e)], the smeared fluctuating band is corresponding to a large $\hbar\Gamma_{CDW} = 1$ eV [64] as a weak damping channel to the plasmon. As the temperature decreases, the band fluctuation becomes smaller, i.e., the fluctuating band tends to be the folding band as a stronger damping channel to the plasmon, which corresponds to the smaller Γ_{CDW} [Figs. 5(c)–5(e)]. In this process, the plasmon energy is getting slightly lower, the height is suppressed, and the linewidth broadens. Close to T_c , with $\hbar\Gamma_{CDW} = 100$ meV, the peak of the plasmon becomes asymmetric [Fig. 5(c)], indicating the interference with the interband transition across the CDW gap.

In the CDW phase, the CDW fluctuation changes into a well-defined back-folding band [shown as Fig. 1(b)]. As the temperature decreases, the E_g increases [33,60] and the

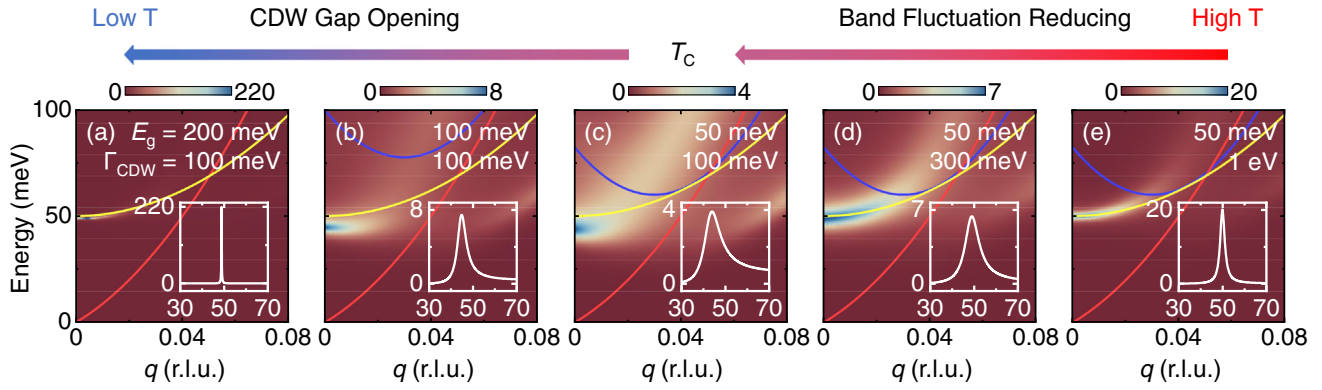


FIG. 5. Loss functions simulated by a Drude-Lorentz model. (a)–(e) Loss functions $\text{Im}[-\epsilon(q, E)^{-1}]$ with different CDW gaps $E_g = 200, 100, 50, 50,$ and 50 meV and interband damping parameters $\Gamma_{\text{CDW}} = 100, 100, 100, 300$ meV, and 1 eV, respectively. The yellow, red, and blue lines highlight the input parameters: energies of a partly screened plasmon, the intraband transitions, and the interband transitions across the CDW gap, respectively. Inset: the line shape of the loss function at $q = 0$. The labels on the horizontal and vertical axes are Energy (meV) and Loss Function, respectively.

interband transitions move away from the plasmon thus reducing the corresponding plasmon damping channel, while the Γ_{CDW} keeps almost constant [Figs. 5(a)–5(c)]. In this process, the plasmon energy slightly increases, but more importantly, the plasmon loss feature becomes much more well defined with narrower linewidth compared with the loss feature at high temperature. Besides, the plasmon dispersion becomes close to zero even negative [Fig. 5(b)]. More simulation data with the continuous evolution can be seen in the supplemental video in the Supplemental Material [40].

The drastic changes in the interband transition damping channel responding to the CDW gap evolution result in the anomalous sharpening of the plasmon feature. Fundamentally, this dramatic response is due to the intrinsic small-gap semiconductor (or semimetal) band structure of the normal phases in $1T\text{-TiSe}_2$, where the interband transitions and the plasmon are close in the energy scale and interfere with each other sensitively [65]. This condition is often not satisfied in regular metal or large-gap semiconductors. This work presents a general framework to understand how the collective electron excitations respond to electron-hole pair excitations in semimetals and small-gap semiconductors and provides possible tunability of plasmons in plasmonic applications [66–68].

The authors would like to acknowledge Prof. E. W. Plummer for his recommendations in the initial stage of this study. This work was supported by the National Key R&D Program of China (No. 2021YFA1400200 and No. 2017YFA0303600), the National Natural Science Foundation of China (No. 11874404 and No. 11974399), and the Strategic Priority Research Program of Chinese Academy of Sciences (No. XDB33000000). V.M.S. acknowledges financial support by Grant No. PID2019-105488GB-I00 funded by MCIN/AEI/10.13039/5011

00011033/. X.Z. was partially supported by the Youth Innovation Promotion Association of Chinese Academy of Sciences.

*These authors contributed equally to this work.

[†]jdguo@iphy.ac.cn

[‡]xtzhu@iphy.ac.cn

- [1] G. Grüner, *Rev. Mod. Phys.* **60**, 1129 (1988).
- [2] X. Zhu, Y. Cao, J. Zhang, E. W. Plummer, and J. Guo, *Proc. Natl. Acad. Sci. U.S.A.* **112**, 2367 (2015).
- [3] F. J. Di Salvo, D. E. Moncton, and J. V. Waszczak, *Phys. Rev. B* **14**, 4321 (1976).
- [4] H. P. Hughes, *J. Phys. C* **10**, L319 (1977).
- [5] J. A. Wilson, *Phys. Status Solidi B* **86**, 11 (1978).
- [6] N. Wakabayashi, H. Smith, K. Woo, and F. Brown, *Solid State Commun.* **28**, 923 (1978).
- [7] M. Holt, P. Zschack, H. Hong, M. Y. Chou, and T.-C. Chiang, *Phys. Rev. Lett.* **86**, 3799 (2001).
- [8] T. E. Kidd, T. Miller, M. Y. Chou, and T.-C. Chiang, *Phys. Rev. Lett.* **88**, 226402 (2002).
- [9] K. Rossnagel, L. Kipp, and M. Skibowski, *Phys. Rev. B* **65**, 235101 (2002).
- [10] F. Weber, S. Rosenkranz, J.-P. Castellan, R. Osborn, G. Karapetrov, R. Hott, R. Heid, K.-P. Bohnen, and A. Alatas, *Phys. Rev. Lett.* **107**, 266401 (2011).
- [11] B. Hildebrand, C. Didiot, A. M. Novello, G. Monney, A. Scarfato, A. Ubaldini, H. Berger, D. R. Bowler, C. Renner, and P. Aebi, *Phys. Rev. Lett.* **112**, 197001 (2014).
- [12] M. Porer, U. Leierseder, J. M. Ménard, H. Dachraoui, L. Mouchliadis, I. E. Perakis, U. Heinzmann, J. Demsar, K. Rossnagel, and R. Huber, *Nat. Mater.* **13**, 857 (2014).
- [13] B. Hildebrand, T. Jaouen, C. Didiot, E. Razzoli, G. Monney, M.-L. Mottas, A. Ubaldini, H. Berger, C. Barreateau, H. Beck, D. R. Bowler, and P. Aebi, *Phys. Rev. B* **93**, 125140 (2016).
- [14] J. A. Wilson, A. S. Barker, F. J. Di Salvo, and J. A. Ditzenberger, *Phys. Rev. B* **18**, 2866 (1978).

- [15] T. Pillo, J. Hayoz, H. Berger, F. Lévy, L. Schlapbach, and P. Aebi, *Phys. Rev. B* **61**, 16213 (2000).
- [16] H. Cercellier, C. Monney, F. Clerc, C. Battaglia, L. Despont, M. G. Garnier, H. Beck, P. Aebi, L. Patthey, H. Berger, and L. Forró, *Phys. Rev. Lett.* **99**, 146403 (2007).
- [17] D. Qian, D. Hsieh, L. Wray, E. Morosan, N. L. Wang, Y. Xia, R. J. Cava, and M. Z. Hasan, *Phys. Rev. Lett.* **98**, 117007 (2007).
- [18] C. Monney, H. Cercellier, F. Clerc, C. Battaglia, E. F. Schwier, C. Didiot, M. G. Garnier, H. Beck, P. Aebi, H. Berger, L. Forró, and L. Patthey, *Phys. Rev. B* **79**, 045116 (2009).
- [19] C. Monney, E. F. Schwier, M. G. Garnier, N. Mariotti, C. Didiot, H. Beck, P. Aebi, H. Cercellier, J. Marcus, C. Battaglia, H. Berger, and A. N. Titov, *Phys. Rev. B* **81**, 155104 (2010).
- [20] E. Möhr-Vorobeva, S. L. Johnson, P. Beaud, U. Staub, R. De Souza, C. Milne, G. Ingold, J. Demsar, H. Schaefer, and A. Titov, *Phys. Rev. Lett.* **107**, 036403 (2011).
- [21] A. Kogar, M. S. Rak, S. Vig, A. A. Husain, F. Flicker, Y. I. Joe, L. Venema, G. J. MacDougall, T. C. Chiang, E. Fradkin, J. van Wezel, and P. Abbamonte, *Science* **358**, 1314 (2017).
- [22] J. van Wezel, P. Nahai-Williamson, and S. S. Saxena, *Europhys. Lett.* **89**, 47004 (2010).
- [23] J. van Wezel, P. Nahai-Williamson, and S. S. Saxena, *Phys. Rev. B* **81**, 165109 (2010).
- [24] J. van Wezel, P. Nahai-Williamson, and S. S. Saxena, *Phys. Rev. B* **83**, 024502 (2011).
- [25] C. Monney, C. Battaglia, H. Cercellier, P. Aebi, and H. Beck, *Phys. Rev. Lett.* **106**, 106404 (2011).
- [26] M. M. May, C. Brabetz, C. Janowitz, and R. Manzke, *Phys. Rev. Lett.* **107**, 176405 (2011).
- [27] C. Monney, M. Puppini, C. W. Nicholson, M. Hoesch, R. T. Chapman, E. Springate, H. Berger, A. Magrez, C. Cacho, R. Ernstorfer, and M. Wolf, *Phys. Rev. B* **94**, 165165 (2016).
- [28] G. Monney, C. Monney, B. Hildebrand, P. Aebi, and H. Beck, *Phys. Rev. Lett.* **114**, 086402 (2015).
- [29] J. M. Bok, J. Hwang, and H.-Y. Choi, *Phys. Rev. B* **103**, 205108 (2021).
- [30] R. Bianco, M. Calandra, and F. Mauri, *Phys. Rev. B* **92**, 094107 (2015).
- [31] A. Wegner, J. Zhao, J. Li, J. Yang, A. A. Anikin, G. Karapetrov, K. Esfarjani, D. Louca, and U. Chatterjee, *Phys. Rev. B* **101**, 195145 (2020).
- [32] C. Monney, G. Monney, P. Aebi, and H. Beck, *Phys. Rev. B* **85**, 235150 (2012).
- [33] P. Chen, Y.-H. Chan, X.-Y. Fang, S.-K. Mo, Z. Hussain, A.-V. Fedorov, M. Y. Chou, and T.-C. Chiang, *Sci. Rep.* **6**, 37910 (2016).
- [34] Y. Miyahara, H. Bando, and H. Ozaki, *J. Phys. Condens. Matter* **7**, 2553 (1995).
- [35] C. Lian, Z. A. Ali, and B. M. Wong, *Phys. Rev. B* **100**, 205423 (2019).
- [36] X. Zhu, Y. Cao, S. Zhang, X. Jia, Q. Guo, F. Yang, L. Zhu, J. Zhang, E. W. Plummer, and J. Guo, *Rev. Sci. Instrum.* **86**, 083902 (2015).
- [37] M. S. Haque and K. L. Kliewer, *Phys. Rev. B* **7**, 2416 (1973).
- [38] K. Pandey, P. Platzman, P. Eisenberger, and E.-N. Foo, *Phys. Rev. B* **9**, 5046 (1974).
- [39] H. Raether, *Excitation of Plasmons and Interband Transitions by Electrons* (Springer, New York, 2006).
- [40] See Supplemental Material at <http://link.aps.org/supplemental/10.1103/PhysRevLett.129.187601> for details about sample preparation, experimental methods, identification of the HREELS features, fitting methods, and calculations, which includes Refs. [41–54].
- [41] P. Lambin, J.-P. Vigneron, and A. Lucas, *Comput. Phys. Commun.* **60**, 351 (1990).
- [42] J. A. Holy, K. C. Woo, M. V. Klein, and F. C. Brown, *Phys. Rev. B* **16**, 3628 (1977).
- [43] V. M. Silkin, E. Chulkov, I. Y. Sklyadneva, and V. E. Panin, *Sov. Phys. J.* **27**, 762 (1984).
- [44] D. M. Ceperley and B. J. Alder, *Phys. Rev. Lett.* **45**, 566 (1980).
- [45] N. Troullier and J. L. Martins, *Phys. Rev. B* **43**, 1993 (1991).
- [46] T. Rohwer, S. Hellmann, M. Wiesenmayer, C. Sohr, A. Stange, B. Slomski, A. Carr, Y. Liu, L. M. Avila, M. Kalläne, S. Mathias, L. Kipp, K. Rossnagel, and M. Bauer, *Nature (London)* **471**, 490 (2011).
- [47] D. Pines and N. Philippe, *Theory of Quantum Liquids: Normal Fermi Liquids (1st ed.)* (CRC Press, Boca Raton, 1966).
- [48] E. Runge and E. K. U. Gross, *Phys. Rev. Lett.* **52**, 997 (1984).
- [49] M. Petersilka, U. J. Gossmann, and E. K. U. Gross, *Phys. Rev. Lett.* **76**, 1212 (1996).
- [50] V. M. Silkin, E. V. Chulkov, and P. M. Echenique, *Phys. Rev. B* **68**, 205106 (2003).
- [51] G. Kresse and J. Furthmüller, *Phys. Rev. B* **54**, 11169 (1996).
- [52] A. Togo and I. Tanaka, *Scr. Mater.* **108**, 1 (2015).
- [53] C. J. Powell, *J. Opt. Soc. Am.* **59**, 738 (1969).
- [54] W. Drube, I. Schäfer, G. Karschnick, and M. Skibowski, *Phys. Rev. B* **30**, 6248 (1984).
- [55] H. Ibach and D. L. Mills, *Electron Energy Loss Spectroscopy and Surface Vibrations* (Academic Press, New York, 2013).
- [56] W. Y. Liang, G. Lucovsky, J. C. Mikkelsen, and R. H. Friend, *Philos. Mag. B* **39**, 133 (1979).
- [57] G. Li, W. Z. Hu, D. Qian, D. Hsieh, M. Z. Hasan, E. Morosan, R. J. Cava, and N. L. Wang, *Phys. Rev. Lett.* **99**, 027404 (2007).
- [58] In the CDW phase, the plasmon line shape is modulated by phonons above 115 K, since the plasmon energy is close to phonons.
- [59] The q_c is defined by the minimum of the momentum where there is no zero point in the real part of the calculated dielectric function. See details in the Supplemental Materials [40].
- [60] C. Monney, K. J. Zhou, H. Cercellier, Z. Vydrova, M. G. Garnier, G. Monney, V. N. Strocov, H. Berger, H. Beck, T. Schmitt, and P. Aebi, *Phys. Rev. Lett.* **109**, 047401 (2012).
- [61] P. Knowles, B. Yang, T. Muramatsu, O. Moulding, J. Buhot, C. J. Sayers, E. Da Como, and S. Friedemann, *Phys. Rev. Lett.* **124**, 167602 (2020).

- [62] C. Monney, E. F. Schwier, M. G. Garnier, C. Battaglia, N. Mariotti, C. Didiot, H. Cercellier, J. Marcus, H. Berger, A. N. Titov, H. Beck, and P. Aebi, *Europhys. Lett.* **92**, 47003 (2010).
- [63] In this simulation, the interband and intraband transition refer to the SPE boundary, but the SPE continuum in the region of large q is not considered.
- [64] The real Γ_{CDW} may be not so large. To emphasize the evolution of the plasmon, we chose such an extreme value.
- [65] E. T. Jensen, R. E. Palmer, W. Allison, and J. F. Annett, *Phys. Rev. Lett.* **66**, 492 (1991).
- [66] Z. Zhu, Y. Zou, W. Hu, Y. Li, Y. Gu, B. Cao, N. Guo, L. Wang, J. Song, S. Zhang, H. Gu, and H. Zeng, *Adv. Funct. Mater.* **26**, 1793 (2016).
- [67] T. Taliercio and P. Biagioni, *Nanophotonics* **8**, 949 (2019).
- [68] S. Cong, X. Liu, Y. Jiang, W. Zhang, and Z. Zhao, *The Innovation* **1**, 100051 (2020).